Productivity Enhancement in Laser Induced Plasma Micromachining by altering the Salinity of the Dielectric Media

ICOMM 2014 No. 93

Ishan Saxena[1] Kornel Ehmann[2] Jian Cao[3]

[1,2,3] *Dept. Of Mechanical Engineering, Northwestern University*

Abstract

Laser Induced Plasma Micromachining (LIPMM), a recently pioneered micromachining process, offers higher material removal rates and greater aspect-ratios of machined features as compared to laser ablation, while preserving its higher resolution and precision as compared with mechanical (tool-based) micromachining processes. LIPMM involves focusing a pulsed laser beam within a transparent liquid dielectric such as distilled water to induce optical breakdown, and is hence greatly influenced by the dielectric's thermo-electrical properties. This study presents a possibility for process improvement by modifying the dielectric medium composition to target higher material removal rates, aspect ratios and other desirable machining characteristics. We report the influence of salt concentration in distilled water, to achieve greater feature depths and material removal rates in surface micro-machining of Aluminum by the LIPMM process. The key results of this study show up to 100% increase in depth at an optimum salinity of 2-4 g/100 ml. Also, the machining characteristics correlate with the plasma generation thresholds for the corresponding salinities.

Keywords: Micromachining, Laser Induced Plasma, Dielectric, Salinity

1. Introduction

Precision micro-texturing over large surfaces has been sought after for various applications like hydrophobicity, bacteria retention, anti-reflective surfaces, friction reduction and other engineered surfaces with desired textures and topography at the micro-scale [1-4]. Many of these applications require multi-material processing, faster processing speeds, and high aspect-ratios. The characteristic sizes of typical micro-features may range from a few microns to sub-millimeter. Short-pulsed and ultra short-pulsed laser ablation is a high-resolution tool-less process for micro-texturing, offering superior resolution, control and precision as compared to mechanical micro-machining as well as other tool-based processes such as micro EDM [5]. However, efficient laser ablation majorly depends on good coupling between the radiation and the material [6], which is based on the selection of wavelength for the material, the reflectivity and absorption coefficient at that wavelength, intensity of radiation reaching the material surface, pulse duration and exposure time [6]. These parameters can significantly control the ablation depth, aspect-ratio and the extent of the heat-affected zones.

Laser Induced Plasma Micro-machining (LIPMM) [7-14] is an efficient alternative mechanism for material removal, as opposed to direct ablation. In LIPMM, the beam is brought to focus inside a transparent liquid dielectric into which the workpiece is immersed. By means of optical breakdown, a plasma plume is formed when the peak intensity at the focal spot exceeds the irradiation threshold for plasma formation. The plasma, which is an opaque, highly localized thermal zone with peak temperature > 5,600 K is then brought in contact with the workpiece to facilitate material removal. Instead of photo-ablation, the mechanism of material removal is a combined effect of mechanical erosion via shock wave propagating radially from an expanding plasma, and thermal vaporization of material in contact with the plasma [15]. This process surpasses the limitations for machining certain materials owing to their optical transmittivity and reflectivity, thereby presenting an opportunity to work with materials having low ablation coefficients, high surface reflectivity and even materials that are transparent to the beam wavelength [7].

Since the effective material removal rate (MRR) in LIPMM is still limited by the peak power and other beam characteristics, the motivation for this study is to explore a method for improving material removal rates and aspect ratios without having to increase the beam power, but instead by altering the dielectric composition via addition of pure NaCl. The proposed modified process would be an efficient, cost-effective and simple alternative to using a higher pulse energy laser, by enhancing the energy density and absorption within the plasma plume, which in turn would lead to higher MRR for the same beam intensity and other beam parameters.

2. Background

2.1. Dielectric Breakdown

Laser induced optical breakdown of transparent dielectrics has been studied by several researchers in the past [16, 17]. Investigations have been done into determining breakdown thresholds, absorption coefficients and life-cycle of laser induced plasma. The breakdown mechanism plays an important role in determining the machining characteristics, because apart from predicting the plasma intensity, it also governs the beam propagation through the plasma plume. The general rate equation of evolution of free electrons in an irradiated medium can be represented by the following equation:

$$\frac{dp}{dt} = \left(\frac{dp}{dt}\right)_{mp} + \eta_{casc} p - gp - \eta_{rec} p^2 \quad (1)$$

Where p is the free electron density in the medium, η_{casc} is the coefficient of cascade ionization, g is the rate of diffusion, and η_{rec} is the coefficient of recombination. Therefore, the terms on the right of equation (1) correspond to the rate contributions due to multiphoton ionization, cascade ionization, electron diffusion outside the plasma, and recombination respectively. Multi-photon absorption takes place when an outer electron absorbs one or more photons to be ejected from its orbit, thereby creating an electron-ion pair. Cascade ionization on the other hand, is the electron-ion pair creation via collision from free electrons which acquire kinetic energy from an incoming photon. In laser induced plasma, for pulse durations greater than 40 fs, the dominant process for electron-ion generation is cascade ionization [18], assuming the presence of seed electrons generated via thermionic effect or presence of impurities. Based on cascade ionization rate, the plasma generation threshold can be approximated by [16]:

$$I_{th} = \frac{cn\varepsilon_0 m^2 \omega^2 \Delta E}{Me^2} \quad (2)$$

where n is the refractive index of the medium, ω is the angular frequency, ε_0 is the permittivity of free space, m and ΔE are the mass and ionization energy of the medium, and c is the speed of light. Moreover, the absorption coefficient (opacity) of the medium influences the fractional intensity reaching the focal volume, as well as the intensity propagating through the breakdown region, governed by equation (3):

$$I(x) = I(0)\exp(-\alpha x) \quad (3)$$

where $I(0)$ is the unabsorbed intensity, α is the absorption coefficient and $I(x)$ is the intensity after traveling through a distance x (absorption length) in the medium. Therefore, the effective plasma generation threshold is the resultant effect of the rate of ionization, and of the absorption coefficient of the medium.

2.2. Influence of Salinity

Due to the availability of constituent Na+ and Cl- ions within a completely dissociated salt solution in distilled water, the effective ionization energy of the medium is reduced, thereby reducing the threshold intensity for plasma generation, and increasing the charge density within the breakdown region. The presence of ions also assists in the multi-photon ionization, which is the dominant mechanism of plasma generation in ultra-short pulses (<100 fs duration), and is an initiator for cascade ionization for longer pulses (>100 fs) [10]. However, dissolved NaCl also influences the attenuation coefficient of the medium, as per the following equation for absorption in solutions, derived from Beer-Lambert's law:

$$\alpha_{sw} = \alpha_w + \alpha_s + b_s \quad (4)$$

Where α_{sw}, α_w and α_s are the absorption coefficients of salt water, pure water and pure salt respectively, and b_s is the scattering coefficient of pure salt. It has been found by researchers in the past, that attenuation coefficient has a linear relationship with salinity [19], and most of it is due to the increased scattering rather than increased absorption. Therefore, the overall effect of salinity on plasma generation in a medium is an interplay of reduced ionization energy and increased attenuation coefficient, which suggests an optimum salinity level for achieving the lowest threshold intensity for plasma generation as well as correspondingly greater feature depths and material removal rates in the LIPMM process. In the past, researchers have observed lower plasma generation thresholds for saline (0.9%, or 9 g/litre) water as compared to distilled water, by a difference of about 10-15%, depending on the pulse duration [9]. However, there still needs to be an investigation into the entire range on salinity levels (up to saturation) with respect to their impact on plasma generation threshold and machining capabilities.

3. Experimental Setup

3.1. Processing Conditions

A commercially available Nd-YVO_4 laser (Lumera Lasers Inc.) with 8 ps pulse duration operating at its second harmonic (532 nm wavelength) was used for LIPMM. The operating pulse repetition frequency was varied between 10 kHz and 50 kHz. The maximum pulse energy obtained was 6 μJ after reflection and transmission losses within the beam delivery system, as measured by an external power meter (Gentec Solo 2(R2)). The Gaussian beam (M^2 < 1.2) was brought to focus with a 25 mm triple-element focusing lens to a diffraction-limited focus of 10.5 μm spot size ($1/e^2$). The substrate was mounted on a 5-axis motion stage with a translation resolution of 10 nm and rotational resolution of 0.0001 degrees. A single-pass micro-channel is created when craters machined by consecutive plasma discharges are overlapped by moving the workpiece at a typical feed-rate of 0.4 mm/s.

Commercially pure (99.9%) reagent grade NaCl was dissolved in distilled water by agitation, to create saline solutions with concentrations ranging from 1 g/100 ml to 35 g/100 ml (salt saturation point of pure water at room temperature). The salt content was measured in a 0.0001 g resolution weighing scale prior to addition to 100 ml water. The pulsed laser beam was brought to focus within the dielectric medium, and stable plasma was observed. This plasma plume was brought in contact with the workpiece (also immersed into the dielectric) to machine features via thermal ablation. Figure 1 shows an image of the plasma plume inside the dielectric while it is not in contact with the workpiece. The laser beam was incident from the top of the image into a beaker filled with distilled water, and the workpiece, immersed into the liquid, was kept below the plasma plume.

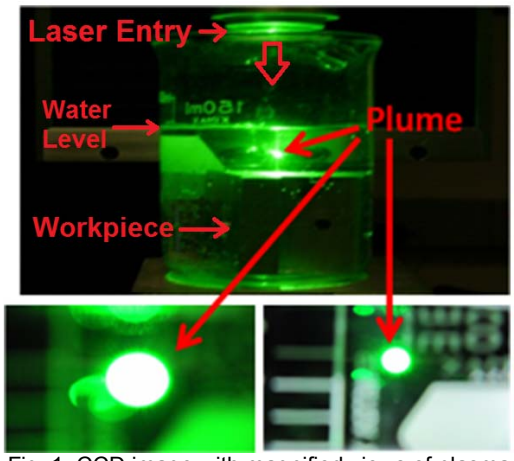

Fig. 1: CCD image with magnified views of plasma plume (beam incident from the top)

2.2. Machining Methodology

A 2% beam splitter was mounted coaxially with the laser beam to send a visual feedback into a high resolution CCD camera for monitoring the machining process and to assist in manually translating the substrate vertically to bring the surface near the focus of the laser beam. A two degree of freedom Goniometer stage was used to adjust the horizontal level of the target surface.

For calculating plasma generation thresholds at different salinity levels, the beam was brought into focus 5 mm below the surface of the dielectric, without any workpiece, and the beam average power was reduced manually until the plasma could not be visually detected on the CCD camera (medium was rendered transparent). For machining with LIPMM, the workpiece was immersed into the dielectric medium and brought into contact with plasma plume at focus of beam (see Fig. 2) to machine channels.

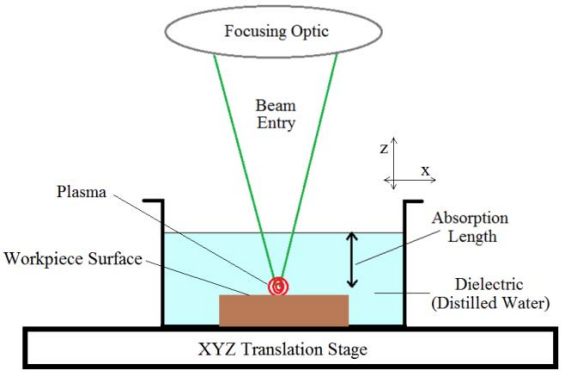

Fig. 2: Schematic of the experimental set-up for LIPMM

2.3 Measurement and Analysis

The depth of micro-channel varies greatly with distance of plasma from the workpiece, which is hard to estimate visually using the coaxially mounted CCD camera. Hence, multiple channels were machined parallel to each other, with different distances of plasma plume from the substrate surface, as shown in Fig. 3 (a). As per the schematic, from left to right, the focal spot was offset vertically up with respect to the surface, to vertically down in the rightmost channel. The step of vertical offset was 50 µm between consecutive channels. This process ensured that the maximum possible depth was achieved was a particular dielectric composition. Thereafter, the deepest channel created was chosen for measurement, as demonstrated in Fig. 3 (b). Post machining, the workpiece was cleaned ultrasonically to eliminate debris. The depth and width of machined channel was measured at three different cross-sections and averaged.

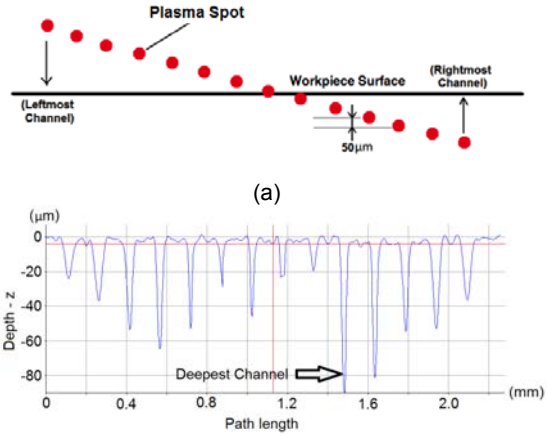

Fig. 3: (a) Schematic representation of methodology of micro-channel machining with different locations of plasma with respect to the workpiece surface; (b) Corresponding micro-channels for the case of 2W beam power and 2 g/100 ml salinity (deepest channel is indicated)

3. Results

3.1. Influence on threshold power for plasma generation

It is essential to understand the relationship between the salinity level of dielectric and the threshold peak power required to generate plasma at the focal spot, in order to understand the role of salinity in machining. The threshold average power was determined experimentally for salinity levels varying from 0 to 35 g/100ml (fresh water to saturation salinity at room temperature), and the corresponding peak power was computed from the average power, as per the following relation:

$$P_{peak} = \frac{P_{avg}}{f_p t_p S}$$

Where, P_{peak} is the peak power, P_{avg} is the average power, f_p is the pulse repetition frequency, t_p is the pulse duration and S is the beam cross-section area at focal spot. The experiment sets were repeated for three different pulse repetition frequencies: 10 kHz, 20 kHz and 50 kHz, see Fig. 4. It can be observed that the threshold power was the lowest at a salinity between the range of 2-4 g/100 ml, for all three pulse repetition frequencies. For these experiments, the

depth of plasma plume underneath the dielectric surface was kept at a constant value of 5 mm, to ensure same absorption lengths.

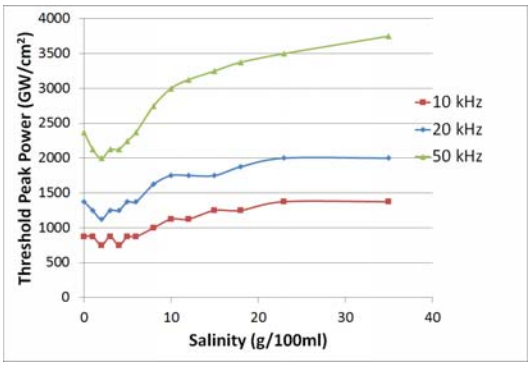

Fig. 4: Variation of threshold peak power for plasma generation with salinity level of water

As shown in Fig. 5, it was observed that the threshold power was also a function of absorption depth. For four salinity levels, the plasma generation threshold was recorded, and was found to increase with absorption depth. This is owing to the fact that intensity reduces exponentially along the propagation path, according to Eq. (3). Also, the rate of increase of the threshold power was observed to increase with salinity, owing to the increase in the absorption coefficient of saline water. At low absorption lengths, the difference between the threshold power in various cases was within 10%. Therefore, to minimize the threshold, the workpiece would have to be placed closer to the surface of the dielectric.

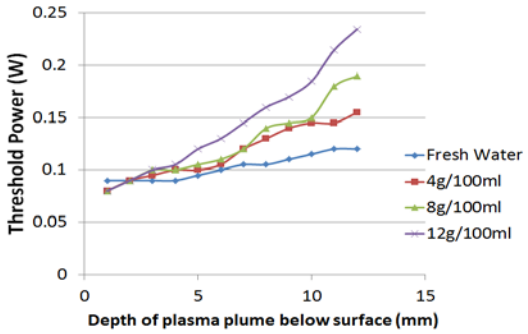

Fig. 5: Threshold power as a function of absorption depth, for different salinity levels

3.2. Influence on machined geometry

The influence of salinity on the machined depth and widths of micro-channels is a function of beam power. Typical channels are shown in Fig. 6, for salinity levels of 0 and 2 g/100 ml.

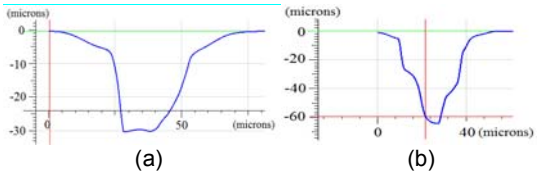

(a) (b)

Fig. 6: Depth profiles of micro-channels made by LIPMM in (a) fresh water, and (b) 2 g/100 ml salinity

3.2.1 Depth

Micro-channel depth was found to increase with increase in salinity, up to 4 g/100 ml, after which the depth steadily reduces for higher salinity levels, see Fig. 7.

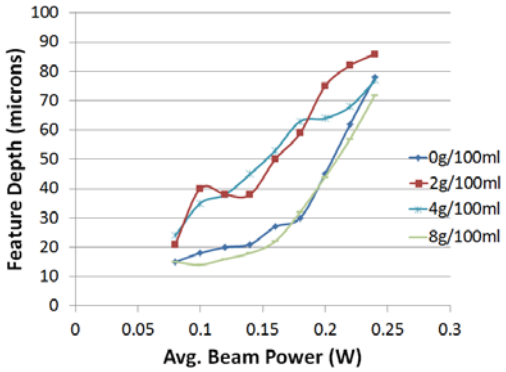

Fig. 7: Micro-channel depth as function of beam power, for different salinity levels

The maximal improvement (up to 100%) in micro-channel depth was observed at 1.5x threshold intensity, as compared to depths obtained by LIPMM in fresh water. However, at near threshold intensities, the depth improvement was less than 20%.

3.2.2 Width

The salinity level had minimum impact on the channel width. The variation in widths measured for different salinity levels was within 5% at threshold intensity, and within 20% at 1.5x threshold intensity with no observable trend, see Fig. 8. This observation strongly suggests that within the focal region, the spatial distribution of energy within the plasma zone is spread more vertically than horizontally. Therefore, the feature width is largely governed by the geometric spot size of the focused beam rather than plasma energy density and strength.

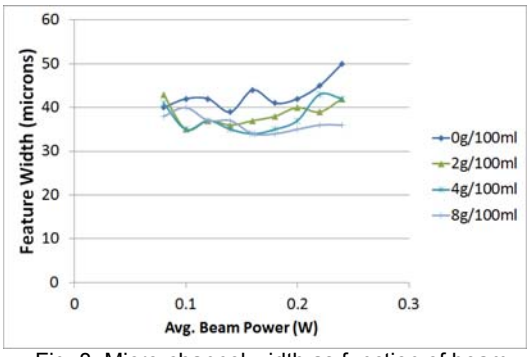

Fig. 8: Micro-channel width as function of beam power, for different salinity levels

3.2.3 Material removal rate

Since the feed-rate of the process was kept constant and the variation in channel widths was insignificant, material removal rate was largely correlated with the machined depths. To determine the material removal rate, the volume of the machined channel was determined by the 3D volume measurement module

within the Alicona infinite focus measurement system, see Fig. 9. The scan area in Fig. 9 (a) represents the portion of the surface which was taken as a reference for computation of ablated volume. Thereafter, the machined volume was divided by the length of the scan segment, in order to obtain the volume of material removed per 100 μm length of micro-channel. Finally, the material removal rate was calculated by taking into account the speed of translation to machine the channel (0.4 mm/s). The rates are plotted as a function of salinity, see Fig. 10. Therefore, it would be logical to conclude that the same optimum salinity value (3 g/ 100 ml) correlates to a higher material removal rate. Similar to improvement in depth, there was a 50-100% improvement in material removal rate at approximately 1.5 times the threshold intensity, while the difference is not as pronounced (< 20%) for near-threshold intensities.

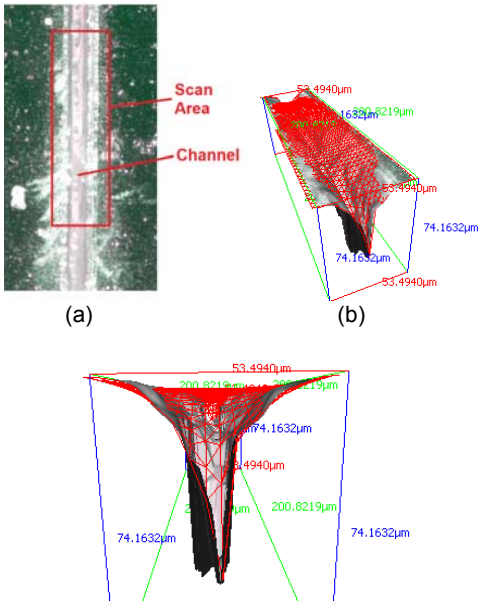

Fig. 9: Volume measurement of 200 μm long segment of micro-channel: (a) Surface image showing scan section, (b) 3-d view of volume measurement, (c) Cross-section view

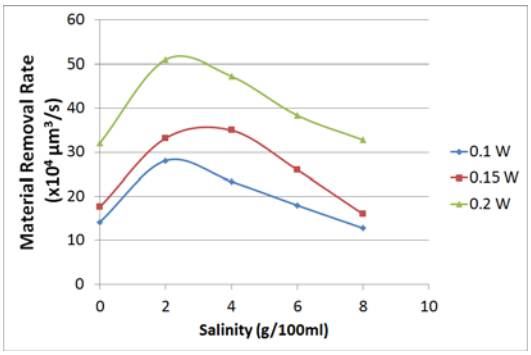

Fig. 10: Material removal rate in micro-channels as a function of salinity in dielectric, for different average beam power

The experimental results also indicate that the spatial enhancement of plasma energy due to added salinity in the medium is more along the vertical direction than horizontal, which leads to higher aspect-ratios in micro-structures.

4. Conclusions

This paper presents an experimental demonstration of the influence of the presence of salinity of the dielectric medium, on machining characteristics of the LIPMM process. The threshold intensity for plasma generation was determined for different salinity levels. Furthermore, aqueous solutions of different salt concentrations were used to machine micro-channels on Aluminum workpieces, and the depths and widths of the channels were measured. The key outcomes in this study are:

1. The lowest threshold intensity for plasma generation was obtained for 2 g/100 ml and 4 g/100 ml salinities.
2. The same salinity concentrations yielded the greatest machined depths of micro-channels.
3. The difference in channel depths was more pronounced (up to 100% increase) for higher energy levels, and less for near-threshold energy levels.
4. The difference in widths was not significant (within 10% range) for salinity levels ranging from 1 g/100 ml to 12 g/100 ml.

This study demonstrates an economically viable enhancement to the recently pioneered LIPMM process, making it more suitable for applications demanding higher aspect-ratio micro-structures and higher processing speeds. However, applying this process modification to a wider range of material processing conditions, a greater experimental and theoretical understanding is required.

Acknowledgements

The authors would like to acknowledge National Science Foundation (awards CMMI #1234491 and #0960776), and DARPA for funding this ongoing research. Research was sponsored by the U.S. Army Contracting Command - New Jersey, Emerging Technologies Contracting Center (ACC-NJ, ET), Benet Laboratories on behalf of the US Army Armament Research, Development & Engineering Command's (ARDEC) Benet Laboratories (BL) and the Defense Advanced Research Projects Agency (DARPA) and was accomplished under Grant Number W15QKN-12-1-0001. The views and conclusions contained in this document are those of the authors and should not be interpreted as representing the official policies, either expressed or implied, of the ACC-NJ, ET on behalf of the ARDEC/BL and DARPA, or the U.S. Government. The U.S. Government is authorized to reproduce and distribute reprints for Government purposes notwithstanding any copyright notation hereon."

References

1. Bico, J., U. Thiele, and D. Quéré, *Wetting of textured surfaces.* Colloids and Surfaces A: Physicochemical and Engineering Aspects, 2002. **206**(1–3): p. 41-46.

2. Nakano, M., et al., *Applying Micro-Texture to Cast Iron Surfaces to Reduce the Friction Coefficient Under Lubricated Conditions*. Tribology Letters, 2007. **28**(2): p. 131-137.
3. Han, P., et al. *Medical Needle Insertion: Effects of Needle Tip and Surface Texturing*. in *Proceeedings of the 6th International Conference on Micro-manufacturing*. 2011.
4. Han, P., K. Pallav, and K.F. Ehmann. *Laser Surface Texturing of Medical Needles for Friction Reduction*. in *Proceedings of the 7th International Conference on Micro-manufacturing (ICOMM 2012)*. 2012.
5. Shirk, M.D. and P.A. Molian, *A Review of Ultrashort Pulsed Laser Ablation of Materials.* Journal of Laser Applications, 1998. **10**(1): p. 18-28.
6. John F. Ready, D.F.F., *LIA Handbook of Laser Materials Processing*. 2001: Magnolia Publishing, Inc.
7. Malhotra, R., et al., *Laser-induced plasma micro-machining (LIPMM) for enhanced productivity and flexibility in laser-based micro-machining processes.* CIRP Annals-Manufacturing Technology, 2013.
8. Pallav, K., et al., *Comparative Assessment of the Laser Induced Plasma Micromachining and the Micro-EDM Processes.* Journal of Manufacturing Science and Engineering, 2013. **136**(1): p. 011001-011001.
9. Pallav, K., I. Saxena, and K. Ehmann, *Laser Induced Plasma Micro-machining Process-Principles and Performance.* International Journal of Machine Tools and Manufacture 2014 (To Appear).
10. Pallav, K., I. Saxena, and K. Ehmann, *Comparative Assessment of the Laser Induced Plasma Micro-machining (LIP-MM) and the Ultra-short Pulsed Laser Ablation Processes.* J. Micro Nano-Manuf. (To appear), 2014.
11. Pallav, K. and K.F. Ehmann, *Feasibility of Laser Induced Plasma Micro-machining (LIP-MM)*, in *Precision Assembly Technologies and Systems*. 2010, Springer. p. 73-80.
12. Pallav, K. and K. Ehmann. *Laser-Induced Plasma Micro-machining*. in *Proceedings of the 2010 ISFA - International Symposium on Flexible Automation*. 2010. Tokyo, Japan.
13. Pallav, K. and K. Ehmann. *Numerical Simulation of the Laser Induced Plasma Micro-machining Process (LIP-MM)*. in *Proceedings of the International Workshop on Micro-factories (IWMF2010)*. 2010. Daejeon, Korea.
14. Pallav, K., *Laser Induced Plasma Micro-machining Process (LIP-MM)*, in *Mechanical Engineering*. 2013, Northwestern University: Evanston, IL.
15. Pallav, K. and K.F. Ehmann, *Laser Induced Plasma Micro-Machining.* ASME Conference Proceedings, 2010. **2010**(49477): p. 363-369.
16. Noack, J. and A. Vogel, *Laser-induced plasma formation in water at nanosecond to femtosecond time scales: calculation of thresholds, absorption coefficients, and energy density.* Quantum Electronics, IEEE Journal of, 1999. **35**(8): p. 1156-1167.
17. Sacchi, C., *Laser-induced electric breakdown in water.* JOSA B, 1991. **8**(2): p. 337-345.
18. Feng, Q., et al., *Theory and simulation on the threshold of water breakdown induced by focused ultrashort laser pulses.* Quantum Electronics, IEEE Journal of, 1997. **33**(2): p. 127-137.
19. Pegau, W.S., D. Gray, and J.R.V. Zaneveld, *Absorption and attenuation of visible and near-infrared light in water: dependence on temperature and salinity.* Applied optics, 1997. **36**(24): p. 6035-6046.